Article

Flow Boiling in Minigap in the Reversed Two-Phase Thermosiphon Loop

Michał Klugmann, Paweł Dąbrowski * and **Dariusz Mikielewicz**

Department of Energy and Industrial Apparatus, Gdańsk University of Technology, 80-233 Gdańsk, Pomorskie, Poland

* Correspondence: pawel.dabrowski@pg.edu.pl; Tel.: +48-604-603-126

check for updates

Abstract: The paper presents the results of experimental investigations of a model of a heat exchanger featuring a minigap, which is perceived as an evaporator for an inverted thermosiphon. The system works with a single component test fluid. The tested evaporator generates pumping power in the test loop in a way similar to the mammoth pump. The tests regarded a module of the heat exchanger, consisting of a hot leg and a cold leg with the width by the length of 0.1×0.2 m, heated by a uniform heat flux. In the tests, the minigaps of 1, 2 and 3 mm were formed. Two fluids, namely, distilled water and ethanol, were tested in the facility. Two-phase flow structures for both working fluids and various operational parameters, together with comprehensive visualization material, are presented. The specifics of pressure changes and its influence on operating parameters and flow structure are discussed.

Keywords: evaporator; solar collector; minigeometry

1. Introduction

The topic of boiling heat transfer in miniscale geometries has received an increase in interest of researchers in recent years. However, most of the works are related to mini- and microchannels and much less to minigaps. The latter are equally important geometries from the application point of view, and they exhibit better thermal properties for certain ranges of the parameters and allow for more comprehensive experimental studies [1]. Particularly of interest are the conditions for flow visualization regarding flat, two-dimensional configurations of flow [2]. Several issues, mentioned in the recent literature, are related to the influence of size [3,4], orientation [5–7] and surface [8–13] structure of the minigap on heat transfer and pressure drop and also to the passive methods [8,14–16].

The heat transfer intensification in passive methods is of interest to authors again [17]. A good example of passive method is the thermosiphon loop, which has been used widely before and is now the focus of research attention again [18]. There were about 200 publications on the topic in 1995 and, 5 years later, only half the number. In 2010, this number rose again to the same level as 15 years ago. Now, about 700 works linked to thermosiphons are published every year and this number is still rising. After all, there is still a need for further studies to understand the thermosiphon heat exchange process and to devise new flow arrangements and configurations.

Thermosiphons, as self-sustaining general flow loops, can be classified according to many criteria [19]. The main classification is related to the number of phases of the working substances, namely: Single-phase (liquid) thermosiphons and two-phase (liquid and vapor) thermosiphons. The use of two-phase thermosiphons gives new opportunities, e.g. the possibility of transporting heat downward, against gravity, in the opposite direction of the natural convection of fluid. There are many methods for forcing spontaneous circulation of the heat transfer fluid in the direction opposite to that of natural convection, among others [20]:

- using capillary forces to pull a cold condensate to the evaporator,
- lifting condensate to an additional reservoir situated above the condenser with the use of saturated vapor pressure and periodical transport of the condensate to the evaporator,
- using the bubble lift,
- periodically forcing the hot liquid through a thermosiphon with the use of vapor pressure.

All systems that use the methods mentioned above can be called reversed thermosiphons. Those kinds of systems give the heat flow from the top to bottom, generally using two-phase flows. The usage of reverse systems results in emerging new research issues [18].

The application of a single-phase (liquid) thermosiphon can be found in several areas. It is mostly used in hot water collection (e.g., solar water heaters [21]) or heat dissipation (e.g., nuclear reactor cooling [22]) but there are also innovative ideas of application such as cold collection and storage of radiative cooling [23]. The application of two-phase (liquid and vapor) thermosiphon is generally wider. It is also used in nuclear systems [24] but in addition, it can be used in the cooling of super-conductors [24], thermal diodes [25], gas turbines [26] or in electronics cooling [16], latent heat thermal storage systems [27], household refrigerator applications [28] and as distillation column reboilers [29]. Reverse two-phase thermosiphons have great potential to operate in solar installations [30] (heat source situated above the heat sink) but due to technical imperfections, these devices have not yet found a wide practical application.

The aim of the paper is to present new research of the reversed thermosiphon with a vapor-liquid lifter. Two working fluids, namely, distilled water and ethanol, were tested. Two-phase flow structures for both working fluids and various operational parameters, together with comprehensive visualization material, are presented. In the case of both fluids, the working fluid operates under sub-atmospheric pressures.

Different aspects of two-phase thermosiphons performance have been investigated over the years.

Dobriansky [19] prepared an extensive review article that summed up the scientific and technical knowledge related to thermosiphons and heat pipes that transmit heat from bottom to top as well as self-sustaining reverse flow loops that transmit heat from the higher part of the system to the lower part. The paper classified the heat and mass transfer processes that take place in general flow loops (thermosiphons or heat pipes) and showed the overall view of the state of the art. In this work, the author presents the principles of operation of sixteen reverse flow arrangements, where most of them are self-sustaining (passive). In seven of the passive loops, the heat transfer was realized with the use of vapor, and, in the remaining five, liquid was used. The work is then summed up with a list of the advantages and disadvantages of presented loops.

C. C. Roberts [20] reviewed nine schemes to achieve liquid pumping over critical distances: (a) Buoyancy bubble pumping, (b) rotating wheel, (c) mechanical pumping using external power, (d) mechanical pumping using internal power, (e) electrohydrodynamic pumping, (f) cascaded heat pipe, (g) oscillating pressure-driven pumping, (h) osmotic heat pipe, and (i) bubble injection pumping. These methods are examples of how to force the spontaneous circulation of the heat transfer fluid in the opposite direction to that of natural convection.

Klugmann et al. [18] presented the research of a reversed thermosiphon with a vapor-liquid lifter and a minigap evaporator of 1 mm thickness gap, working with distilled water. The pulsatile mean of the system operation was described, as well as the way of system self-adjustment to the varying heat fluxes. Some flow visualizations were presented.

Several works, published in recent years, are focused on developing microchannel geometries in a passive system, i.e., thermosiphons. Some authors have also worked on mini- and microgaps that are not necessarily implemented in the thermosiphons but are worth to mention here.

Alam et al. [4] focused on flow boiling experiments where deionized water was used as a working fluid. They tried to determine the most effective and efficient range of microgap dimensions based on heat transfer and pressure drop performance in a silicon microgap heat sink. The experiments were conducted for ten different microgap depths from a range of 80 to 1000 μm. In addition to thermal

measurements, a high-speed visualization of flow in gap was conducted. The results of this study showed that various flow patterns occur for different microgap sizes. Due to the development of partial dryout, the microgap is ineffective below 100 μm. Moreover, the wall temperature reaches higher values for a fixed heat flux when microgap size increases above 500 μm. In addition, the increase of microgap size results in a decrease of pressure drop, which is not surprising, but also a decrease of pressure fluctuations, which is a desirable phenomenon. However, wall temperature and its fluctuations increase with the increase of the gap size. It was only for the minigap below 500 μm that a significant impact on the heat transfer coefficient was observed.

With regard to these geometries, several works describing the characteristic "M-shape" distribution characteristics related to heat exchange and vapor quality have been published in recent years.

Bar-Cohen et al. [31] presented a comprehensive literature review work where they analyzed the heat transfer data for two-phase flow of refrigerants and dielectric liquids in microchannel/microgap heat sinks. The authors used the inverse calculation of IR images of a heated microgap channel wall and the thermal measurements for single minichannel to identify the existence of a characteristic M-shaped heat transfer coefficient vs vapor quality. Other researchers [32] observed similar M-shaped distributions for small diameter channels.

When minichannels or minigaps are being applied in heat exchangers (also, for example, in a thermosiphon circuit), the issue of even distribution of a working fluid in a complex flow system gains importance. This is an issue of the so-called flow maldistribution.

Dąbrowski et al. [33] accomplished hydrodynamic studies in a minichannel plate heat exchanger which contained 51 parallel minichannels. The channels' cross-section was rectangular with a constant width and various depths, which resulted in various hydraulic diameter of channels (461, 574, 667, and 750 μm). All the channels were connected by a common trapezoidal inlet and outlet manifold. The studies were to check the potential of a minichannel heat exchanger as an evaporator in a solar thermosiphon installation with particular emphasis on flow distribution. The flow maldistribution was measured by observing the single-phase flow at the moment of filling the model heat exchanger. Authors noticed the channel blockage phenomenon that they described and tried to systematize by classifying them into two types. The authors described the dependency of the mass flow rate and the channels' cross-section dimensions on flow maldistribution and blockage mechanism. The experiment showed that there is a critical mass flux below which the phenomenon starts to be significant.

As it has been shown in the literature review above, there are several works dealing with thermosiphons or reversed thermosiphons, as well as works that describe boiling in minigap heat exchangers. However, there are no works that merge those two issues and describe the heat exchange in the minigap evaporator in the reversed thermosiphon. This work is intended to contribute to the current state of knowledge in this area.

The aim of the paper is to present the new research on reversed thermosiphons with vapor-liquid lifters. Two working fluids, namely distilled water and ethanol, were tested. Two-phase flow structures for both working fluids and various operational parameters, together with comprehensive visualization material are presented. In the case of both fluids, the working fluid operates under sub-atmospheric pressures.

2. Materials and Methods

The facility developed for the needs of the present research is presented in Figure 1.
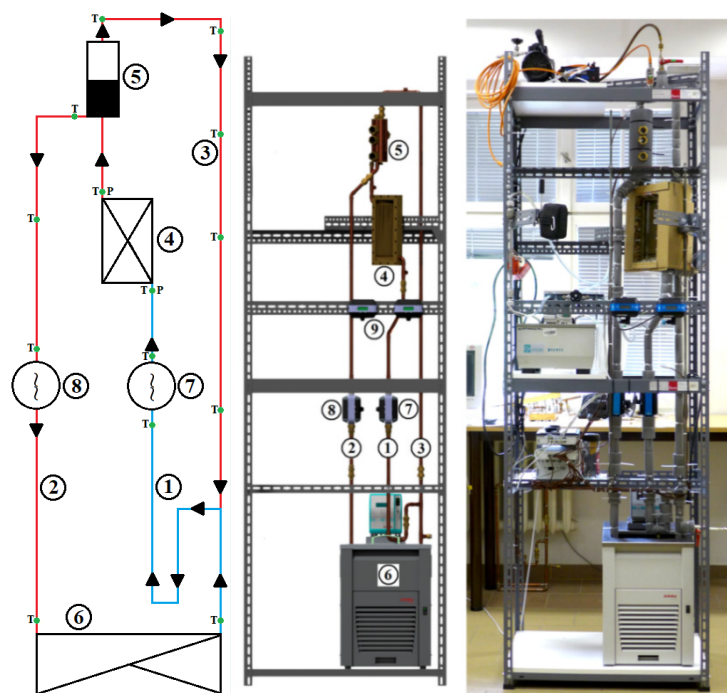
Figure 1. Scheme, model and photo of experimental facility: 1—cold (inlet) liquid pipeline, 2—hot (outlet) liquid pipeline, 3—hot (outlet) vapor pipeline, 4—minigap evaporator, 5—liquid-vapor separator, 6—condenser, 7—inlet ultrasonic flowmeter for cold liquid pipeline, 8—outlet ultrasonic flowmeter for hot liquid pipeline, 9—display, T—thermocouple, P—pressure transmitter.

The experimental facility is an inverted thermosiphon working with a single working fluid which changes phase in the evaporator. The heat and mass transport takes place between the evaporator and the condenser. An evaporator is located 1.35 m above the condenser. The evaporator (4) is the main, replaceable test section. It was designed as a single plate with a heat exchange surface of 0.1×0.2 m, made of brass. A 1, 2, or 3 mm-thick minigap was arranged. The cover is transparent in order to make simultaneous registration of flow structures along with measurements. The heat is supplied to the evaporator (4) by means of a water circuit, provided by a thermostat–circulator. Hot water flows on the opposite side of the exchanger's plate (and minigap) in the co-current configuration. The thermostat ensures the heating water temperature adjustment with an accuracy of 0.1 °C. The working medium flow on the minigap side occurs in the way of natural circulation. The inlet and outlet manifolds of minigap are arranged in trapezoidal (Z-type) design.

In the research, the authors strived to meet the criterion of a constant temperature difference between the wall and the working fluid. On the side of the heating water, the constant wall temperature was ensured by its massiveness (thickness 9 mm) and large water volume of the thermostat (16 dm^3), which resulted in large thermal capacity and inertia in relation to the working medium in the minigap. On the minigap side, the working medium aims to maintain a state of two-phase flow along the entire length of the section. Altogether with a slight pressure drop, it gives a constant fluid temperature equal to the saturation temperature.

The condenser (6) was a copper coil placed in a water bath directly in the thermostat. Water in the thermostat was constantly mixed. Its temperature can be regulated, in the full range of the liquid state, with an accuracy of 0.1 °C. Over the evaporator (4) a separator (5) was located. It receives a working medium in a two-phase state, where its transport takes place on the principle of a steam liquid lifter (similarly as in the mammoth pump). After a part of the two-phase mixture is delivered to the separator (5), the liquid phase flows gravitationally to the bottom of the separator (5) and then, further, down to the pipeline (2) leading to the condenser (6). The vapor flows through a second pipeline (3) in the upper part of the separator (5) and also goes to the condenser (6), partially condensing along the

pipeline (3). In the condenser (6) heat is removed and the working medium is cooled down to the initial temperature. So, it reaches the outlet of the condenser (6) in a completely liquid state.

To control the heat balance and the heat transport process, the installation was equipped with temperature sensors (T-type thermocouples) at all key points as well as at the length of the pipelines. The mass flow of the working medium (ultrasonic flow meter Titan Atrato 740-V10-RD) is measured on the evaporator's inlet pipeline (7) and on the liquid drainage pipeline (8) from the separator (5). The mass flowrate in the vapor pipeline (3) is estimated based on the balance of the two above indications. At the inlet and outlet of the evaporator (4), a pressure measurement (vacuometers Peltron NPXG 1) proceeds. In addition, the temperatures and flowrate of water in evaporator's heating circuit are recorded. Twelve temperature measurement points are located in the evaporator's wall for determining the local heat transfer coefficients (see Figure 2). Through the transparent evaporator's cover, the two-phase flow structures are registered using a Panasonic Lumix LX7 camera. It is an equipment of a popular class, however, it has the ability to record video sequences in FullHD resolution (1920 × 1080) at exposure times up to 1/20,000 s (50 milliseconds). The visual material serves for qualitative analysis and helps in phenomena interpretation. Visual material is not used to obtain quantitative data yet. The schematic view of a minigap plate without a transparent upper cover (minigap closing) and non-transparent bottom cover (heating section closing) is shown in Figure 2.
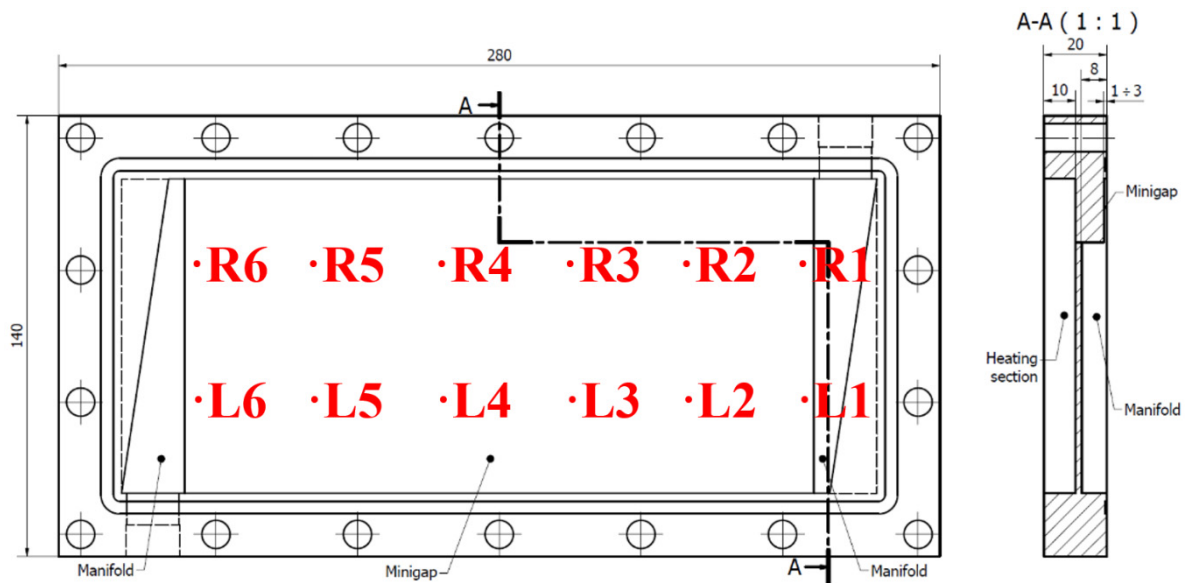

Figure 2. Schematic view of the test section—minigap heat exchanger: L1–L6—left temperature measurement points in the wall; R1–R6—right temperature measurement points in the wall.

The test rig was equipped with 15 of type T class 1 thermocouples that were mounted directly into the flow of the working fluid. The measurement tolerance was ±0.5 K. The flowrate of liquid at the cold and hot pipelines was measured by Atrato AT740 ultrasonic flow meters with the maximum measurement range of 3.33×10^{-8} m^3/s–8.33×10^{-6} m^3/s, with the tolerance of < ±1% and repeatability of ±0.1% of the measured value. At the inlet to flowmeters, working fluid temperatures were measured so the mass flowrate could be calculated knowing the exact density of a fluid. The pressures at the inlet and outlet of the minigap's manifold were measured by Peltron NPXG 1 (Pelltron Towarzystwo Produkcyjno Handlowe sp. z.o.o.; Wiązowna; Poland) vacuometers with the maximum range of applicability of −100 to 0 kPa and tolerance of ±0.1% of the measured value.

The heat to the evaporator is supplied using a water circuit, where the temperature and flow of the water can be regulated in the thermostat. The assumption is to obtain the boiling structures in the minigap which can push the liquid upward into the separator (5) located above the evaporator. It is a liquid transport mechanism similar to those found in airlift (mammoth) pumps. In the separator,

a liquid part of the test fluid flows to the condenser through a pipeline (2) at the bottom of the separator, while the vapor part goes to the pipeline (3) at the top of the separator and further goes to the condenser through the second tube.

The amount of heat given off by the heating water in the evaporator is balanced with the amount of heat removed in the condenser. Lowering the temperature of the evaporator's heating water is the basis for determining the incoming heat flowrate. Similarly, on the condenser side, an increase in the temperature of the cooling water was observed. So ultimately the balance is based on a simple single-phase heat transfer. This is burdened with an error resulting from heat losses. Therefore, additional temperature measurement points were placed along the entire length of the pipelines to determine heat loss through insulation. Because of the complicated construction, it is not possible to insulate the entire evaporator. In particular, the transparent cover must be exposed. Therefore, the heat losses in the evaporator were calculated analytically. Convective heat exchange and thermal radiation were considered.

The system can also work in a two-phase mode without boiling when air is delivered from outside to the open circuit.

The experiment was designed as:

- reversed thermosiphon with a vapor-liquid lifter,
- distilled water and ethanol,
- single-phase test fluid,
- minigap evaporator of 1, 2, or 3 mm thickness and a surface of 100×200 mm,
- convective heating or run using externally pumped air.

The heat was supplied by a hot water circuit.
The following aspects were analyzed:

- inlet and outlet temperature distributions over time in the evaporator,
- inlet and outlet temperature distributions over time in the condenser,
- mass flowrate distribution over the time on liquid and vapor outlets of a separator,
- temperature distribution over the time on liquid and vapor outlets of a separator,
- temperature differences as a function of heat flux supplied to the minigap.

Additionally, the visualizations of the separator's work and the minigap boiling structures were conducted, the example of which is presented in Figure 3.

The following ranges of testing conditions were taken into consideration: Vapor quality 0.00–0.82, heat flux 2500–15 000 W/m^2, mass flux 0–35 kg/m^2·s, absolute system pressure 30–60 kPa.
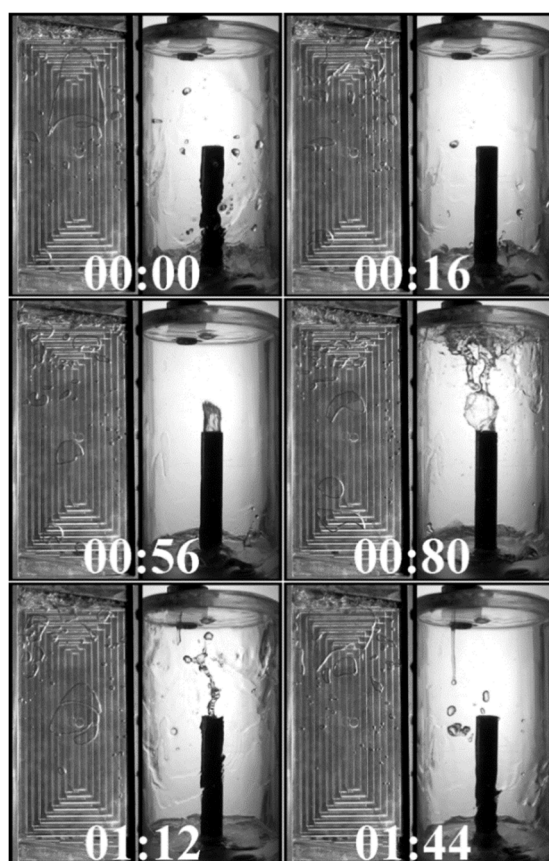
Figure 3. Visualization of the vapor lifting of liquid (one working cycle of the evaporator–separator system); the vapor bubble enters the outlet manifold and pushes out the column of boiling liquid after 0.56 seconds.

3. Results

3.1. The Filling Height of Separator's Pipe

The filling height tests were carried out, keeping the remaining parameters of the system working as constant as possible. As described in the literature review, it is not easy due to their inter-correlations, and also because of the tendency of a system to its dynamic self-regulation. Nevertheless, the parameters of heat supply in the evaporator, the heat removal in the condenser and system pressure, were kept constant. The key factor in the operation of the system is the presence of the test fluid in the separator's tube because, from there, it is pushed out by the vapor bubbles generated in the evaporator. The authors made the experiments with the filling level, which not provides the fluid in the separator's tube. The thermosiphon with such filling level works very poorly or works not at all. That is the reason the authors started to consider the effect of filling height on the thermosiphon's work from the moment when the liquid reached the bottom part of the separator's tube. The filling height h was expressed in a percentage—as the ratio of the height of the liquid column in the separator's tube to the total length of the tube—thus, at the same time, the ratio of the current volume of a liquid in the separator's tube Vi to the maximum volume of liquid when the separator's tube is completely filled $Vmax$ (Equation (1)). It was measured when thermosiphon does not operate, just before supplying the heat to the evaporator. The minimum filling height was 0%, i.e., the condition when the liquid is just before the separator's tube. The next 6 filling heights were in the range of 0–100%. The filling height of 100% was the entirely sunk separator's tube. In the case of the last two measurement points, the liquid level in the installation

reached above the outlet of the separator's tube (it was entirely sunk in the liquid and some liquid started to pour into the separator) —these points are described as >100%.

$$h = \frac{V_i}{V_{max}} \tag{1}$$

The influence of the filling height on the thermosiphon's operation can be analyzed in two ways in relation to mass transfer efficiency and in relation to heat efficiency. Figure 4 shows the mass flux of the test fluid as a function of filling height for the two sizes of the minigap. Figure 5 shows the amount of heat received in the evaporator as a function of the filling height. The mass flux G and heat flux Q were described by Equations (2) and (3), respectively.

$$G = \frac{m}{A_1} \tag{2}$$

where m is mass flowrate of a working medium in the evaporator and A_1 is the cross-section area of the minigap (0.1 m × minigap's depth).

$$Q = \frac{q}{A_2} \tag{3}$$

where q is the heat received by the working medium in the evaporator and A_2 is the area of the minigap (0.1 × 0.2 m).
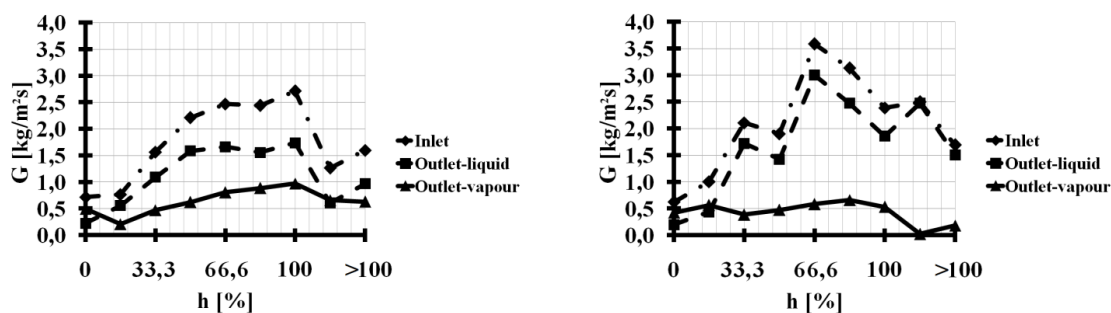

Figure 4. The mass flux of the test fluid at the inlet to the evaporator and at the separator outlets as a percentage function of the filling height: **Left**—minigap 2 mm; **right**—minigap 3 mm.
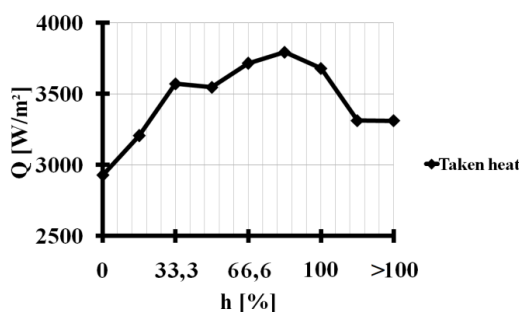

Figure 5. Heat flux delivered to the evaporator as a function of the percentage filling height, minigap 2 mm.

It can be seen that the trend of curves at both approaches is similar, and both curves achieve a distinctive maximum in a certain range of average filling heights. As expected, resulting from the principle of operation of a vapor-liquid lifter, the worst case appears when the separator tube is empty or is filled to a small level. However, contrary to expectations, the mass flow did not stop and there was also heat transport. Importantly, in quantitative terms, both values did not change proportionally. This is because a significant (3.5 to 6 times) reduction in the mass flow of the test fluid through the

evaporator causes much higher vapor qualities (see Figure 6), and the domination of the vapor phase in heat transfer.
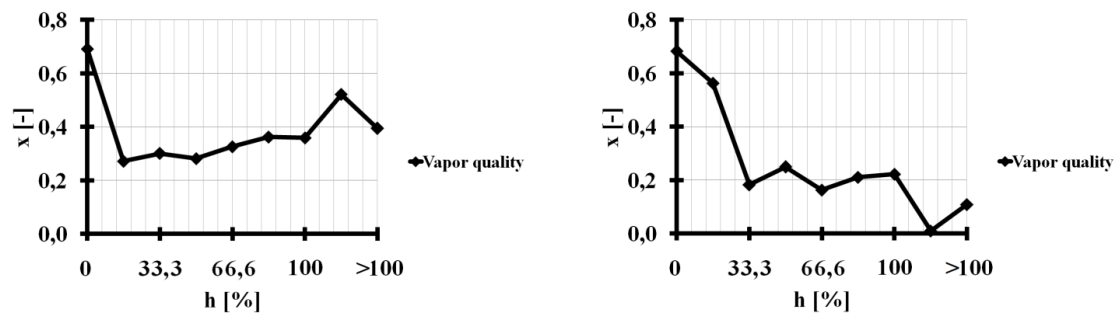

Figure 6. Vapor quality at the outlet from the evaporator as a function of the percentage filling height; **left**—minigap 2 mm; **right**—minigap 3 mm.

The vapor quality *x* was calculated using Equation (4).

$$x \; = \; \frac{m_v}{m_v + m_l} \tag{4}$$

where m_v is the mass flowrate of vapor calculated as a difference of mass flowrates indicated by an inlet ultrasonic flowmeter for the cold liquid pipeline (7) and the outlet ultrasonic flowmeter for the hot liquid pipeline and m_l is the mass flowrate indicated by an inlet ultrasonic flowmeter for the cold liquid pipeline (7).

For the filling heights, at which the vapor lifting of the liquid is already working normally, the vapor quality stabilizes at a certain level, depending on the system pressure. Figure 7 shows how the generation of vapor in minigap looks like at certain filling levels.
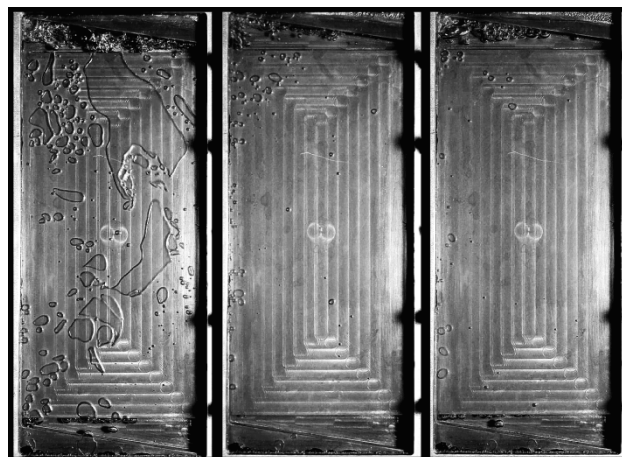

Figure 7. Increased generation of vapor along with a decrease in the mass flow rate of the test fluid resulting from the insufficient efficiency of a vapor-liquid lifting (water, minigap 1 mm): **Left**—filling = 16.6%; **middle**—filling = 100%; **right**—filling > 100%.

In general, an excessive system filling makes the conditions of mass and heat transport worse, but the differences are not as important as in the case of a test fluid shortage. The vapor lifting of the liquid also works when the separator's tube is completely sunk.

3.2. The Influence of the Minigap Height

Visualizing investigations have shown that the reduction of the minigap height leads to an increase in the boiling process intensity and, as a consequence, to higher vapor qualities. This is reflected in

the system efficiency—heat transport and mass transport—but the relationship isn't linear. From the author's own research and literature reports, the effectiveness of heat removal from the minigap wall depends on the vapor quality according to the M-shape curve (Figures 18 and 19), the vapor quality is also important for the efficiency of vapor liquid lifting, and thus, a complex relationship results.

Figure 8 shows the boiling of water in the evaporator with three various minigaps. It is clearly shown that the increase of minigap thickness reduces the number of bubbles generated.

Figure 8. The intensity of the boiling process for three minigap thicknesses and for the same filling height (water): **Left**—1 mm, **middle**—2 mm, **right**—3 mm.

The minigap thickness is also important for the occurrence and intensity of the maldistribution phenomenon along with accompanying phenomena, such as reversed flows.

3.3. The Influence of the Heat Supplied to the Evaporator

It should be kept in mind, that the heat supplied to the thermosiphon of the described design is used in two ways: (a) It is transported and discharged in a condenser, which is the basic function of the system, (b) it produces the pumping power by generating vapor bubbles, so it is partially converted into mechanical work. Thus, the heat flux supplied to the evaporator and removed later in the condenser as well as the mass flux of the test fluid in the system increase proportionally for the balanced conditions of system operation.

The system is balanced when all the heat transferred in the evaporator, after subtracting a small part converted into mechanical work, is transferred to a condenser. In other words, when the condenser is able to cool the test fluid to its initial temperature. The system can become unbalanced in two cases:

- When the heat removed in the condenser is insufficient in relation to the amount of heat taken in the evaporator. As a consequence, the system pressure increases along with the saturation temperature of the test fluid. As a result, the boiling process in the minigap shifts towards flow structures with lower heat-receiving efficiency. The system operating point automatically sets itself at the level at which the condenser capacity is already sufficient. If this is not possible, the pressure increases continuously and the work of the system expires.
- When the heat transfer potential of the condenser is higher than the heat supplied in the evaporator. Then, the excessive cooling of the test fluid causes a decrease in the system pressure and saturation temperature. The consequence is an increase of minigap wall superheating and an intensification of the boiling process.

The case of a balanced system is illustrated in Figures 9 and 10. It can be seen that the working fluid is being cooled in the condenser to its initial temperature.
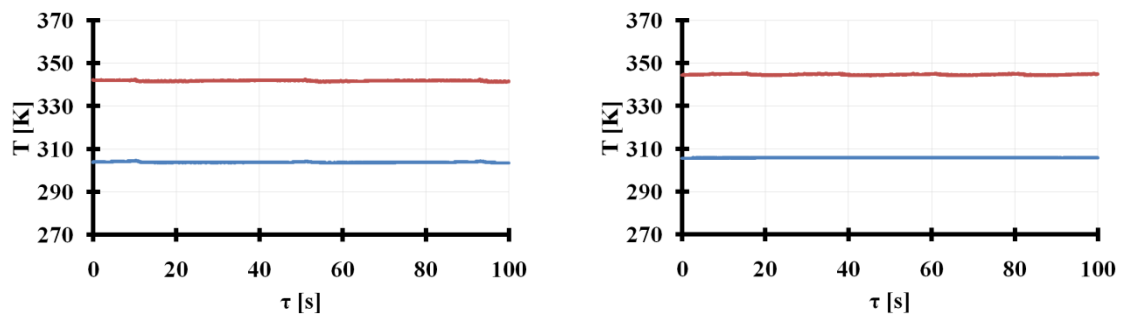
Figure 9. Temperatures in evaporator (blue (lower) —inlet, red (higher)—outlet) for average heat flux supplied to the minigap: **Left** = 7.6 kW/m^2; **right** = 14 kW/m^2 [18].
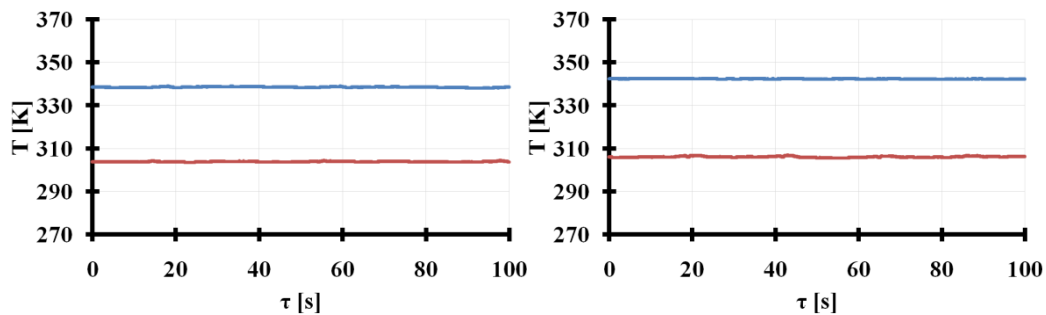
Figure 10. Temperatures in condenser (blue (higher)—inlet, red (lower)—outlet) for average heat flux supplied to the minigap: **left** = 7.6 kW/m^2; **right** = 14 kW/m^2 [18].

Figure 11 shows how the heat flux supplied to the minigap wall influences the average mass flux in the system (in this case—the liquid on the evaporator's inlet), for three minigap dimensions.
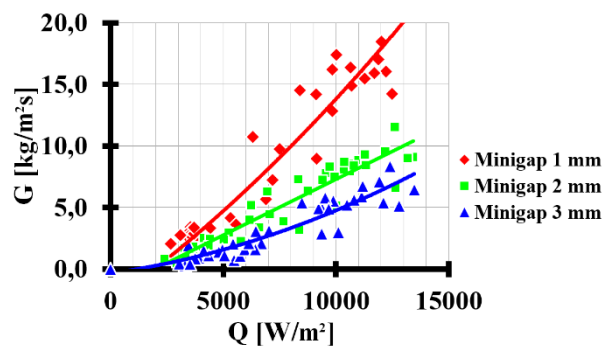
Figure 11. Mass flux of the test fluid (on evaporator's inlet) as a function of heat flux.

The expected increase in the mass flux is visible along with the increase of the heat flux. The influence of the minigap thickness is also visible—the efficiency of the vapor lifting of the liquid seems to increase with its decreasing thickness. This is confirmed by the visualization shown in Figure 8—decreasing the thickness of the minigap leads to the intensifying of the boiling process.

In order to obtain wider information, apart from the analysis of mean values, we also analyzed the distribution of the important thermosiphon operation parameters over time.

Figure 12 shows the distribution of the test fluid mass flux at the evaporator's inlet and on the separator's outlet (in the liquid pipeline) and Figure 13 shows the distribution of the temperature on the separator's outlet over time. A characteristic, pulsating way of system operation demonstrates itself here. It results from the way of a steam liquid lifter works. The amount of vapor coming from the evaporator to the separator's tube must be sufficient to push the portion of the test fluid out from the tube. The duration of the "vapor collecting" cycle depends on the intensity of the evaporator operation, but does not increase linearly together with the vapor quality at its outlet. In addition,

except for vapor, a sufficient portion of liquid to be transported is required, so too-high vapor qualities are not appropriate. The visualization of a separator's single operation cycle (which, together with the evaporator, is a steam liquid lifter) is shown in Figure 3. At the moments of ejection, the fluid from the separator's tube corresponds to the peaks in Figures 12 and 13. The most advantageous ratio of steam to ejected liquid occurs at vapor quality $x = 0.1$, hence the appearance of the distribution in Figure 20.
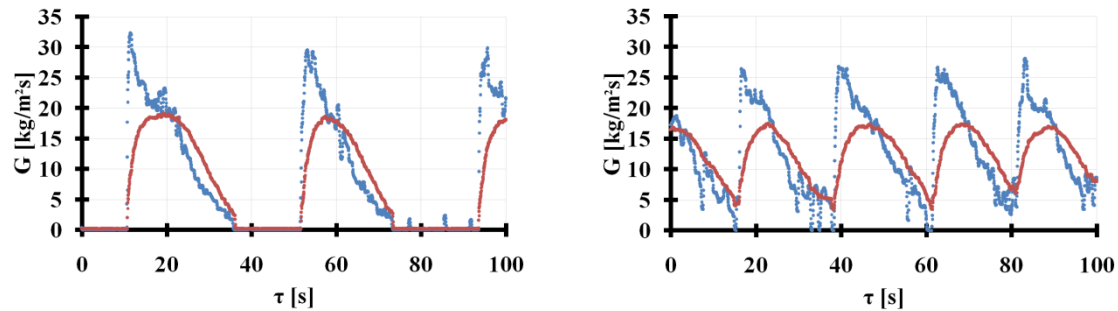

Figure 12. Mass flow rate: blue—at evaporator inlet, red—at separator outlet (liquid pipeline) for average heat flux supplied to minigap: **left** = 7.6 kW/m^2; **right** = 14 kW/m^2 [18].
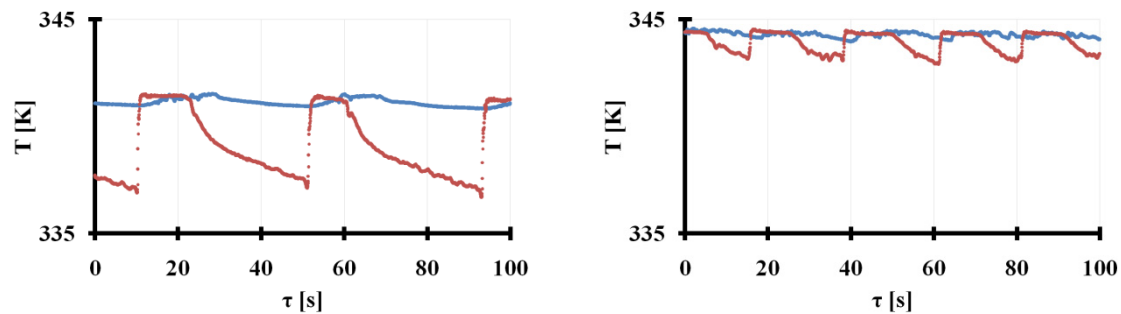

Figure 13. Temperatures on the separator's outlet. Blue—liquid pipeline, red—vapor pipeline for average heat flux supplied to the minigap: **left** = 7.6 kW/m^2, **right** = 14 kW/m^2 [18].

When comparing two different heat flux densities applied to the evaporator, it can be seen that the maximum values differ only slightly. However, proportionally to the increase in the heat flux, the number of operating cycles (the number of eruptions of the test fluid from the evaporator to the separator) increase. This is how the circuit automatically adapts itself to the amount of heat to be transported. Of course, stable work, with a fixed number of cycles per time, requires the balanced conditions of system operation. To some extent, it can automatically achieve this state by reducing or increasing the system pressure, which has a direct impact on the boiling process.

The temperature distribution on the outlet from the separator (liquid and vapor) shows the same cyclic character. It is worth noting that, despite this variability of test fluid temperatures at this point, the inlet and outlet temperatures in the evaporator and condenser remain almost perfectly fixed over time.

3.4. The Influence of the System Pressure

As mentioned above, lowering the system pressure increases the heat demand in the evaporator, because it leads to the lowering of the saturation temperature and, hence, to increased superheat of the minigap wall. It is seen in Figure 14. Figure 15 shows the impact of pressure on bubble growth.
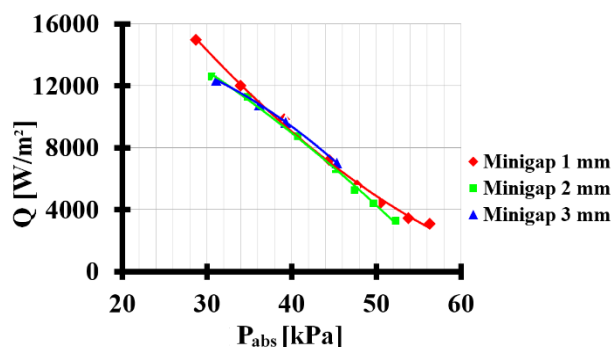
Figure 14. The heat taken over from the minigap wall as a function of absolute pressure.
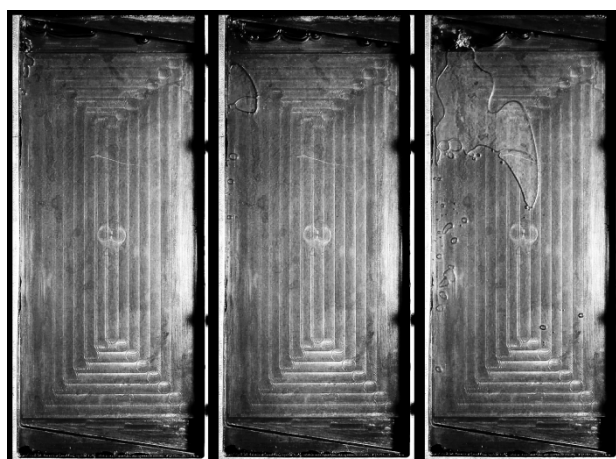

Figure 15. The influence of absolute pressure on vapor bubbles growth (water, minigap 1 mm): **Left** = 61 kPa, **middle** = 54 kPa; **right** = 49 kPa.

Contrary to what may seem, a simple adjustment of the thermosiphon efficiency by changing the system pressure is not possible in a wide range. It results from the above-mentioned fact of the automatic adjustment of the system to the thermal equilibrium state. The final system pressure and flow structure are the derivatives of this state.

This is well illustrated by the case of dry-out, shown in Figure 16. For the conditions of the presented experiment, it's possible to obtain this phenomenon by a significant reduction of the system pressure. It is temporary and an extremely unstable state due to the tendency of self-regulation of the system. It lasts for several dozens of seconds after which it automatically terminates. The mechanism is as follows: Complete evaporation of the liquid in the minigap causes the vapor-liquid lifting mechanism to cease, and also the flow of the test fluid stops immediately. Then the remainder of the liquid from the separator flows gravitationally to the condenser, which causes the cold content of the condenser to be pushed into the evaporator's inlet. The evaporator fills with the cold test fluid and then the boiling process starts again. The intense heat flow into the system causes the system pressure to increase—thus a new operational point develops.

This is another very interesting aspect of the self-regulation of the system—in operating conditions, in which the large wall superheat may occur, this effect protects against burn-out and associated failure.
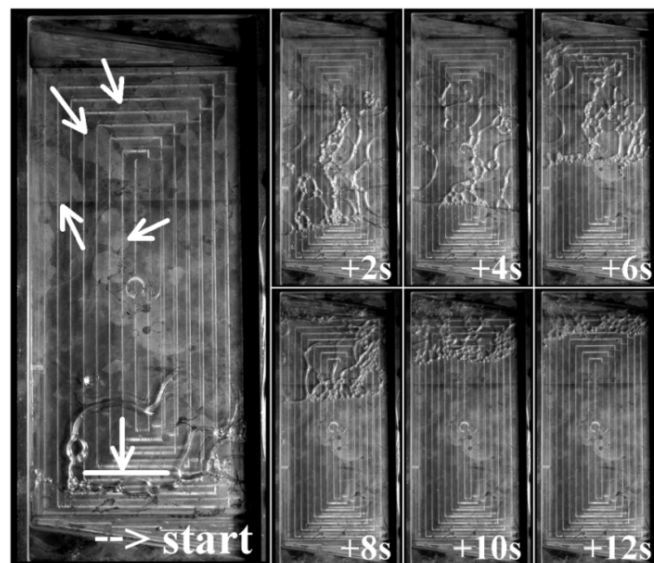
Figure 16. Dryout and subsequent inflow of cold liquid from the condenser—its initial level is marked on the "start" picture; the places where the liquid film dries on the wall (brighter areas) are marked by arrows.

3.5. The Specifics of the Two-Phase Flow

3.5.1. The Adiabatic Flow of the Water-Air Mixture

As a reference variant, used to calibrate the system, an adiabatic air-water flow was used. By supplying air from an external source to the "side entrance" of evaporator's inlet and keeping the circuit open into the atmosphere, the circulation of the test fluid can be obtained. Also, the heat will be transported when supplied to the evaporator. The evaporator in this configuration provides pumping power in accordance with the principle of operation of the classic mammoth pump. Although the flow of the test fluid in the evaporator and in the separator's tube is formally two-phase, the medium does not evaporate. Therefore, the efficiency of heat removal in the evaporator is at the level of forced convection in a single-phase turbulent liquid flow. The flow structures for three different air streams injected into the system and the resulting average mass flow rates of the fluid are shown in Figure 17. Due to the lack of evaporation, the mass flow rates at the evaporator inlet and at the liquid outlet pipeline of the separator are equal. The vapor pipeline in this mode of operation is inactive.

Figure 17. Adiabatic flow of air-water mixture (three flow intensities for different air loads): **Left** = 8.73 kg/m^2·s; **middle** = 26.36 kg/m^2·s; **right** = 45.20 kg/m^2·s.

3.5.2. Flow Boiling

In this case, the impulse forcing the flow is not supplied from the outside, but it is generated in the evaporator itself by the vapor bubbles. In this situation, the system must work in closed-loop (otherwise there would be a loss of a part of the test fluid in the form of vapor). For liquids such as ethanol or water, the under-pressure is required. The resulting flow structures are indeed the boiling structures. Contrary to what might seem, it is difficult to clearly associate specific flow structures with the highest efficiency of thermosiphon work. This results from the complex nature of system work and mutual interactions between various parameters, which is confirmed in [4]. The flow structures that are best from the point of view of heat transfer do not have to exactly coincide with the flow structures that are the best for mass transport. From the point of view of mass transport, the vapor phase is only needed to force the flow of liquid in the separator's tube, while the further flow of the fluid from the separator to the condenser is much more efficient through the gravitational flow of the liquid than through the vapor flow. It follows that relatively low vapor quality values are preferred, with the predominant proportion of the liquid phase. This is confirmed by the observations —effective circulation of the test fluid in the system already occurs under the sub-cooled boiling conditions, with a very modest generation of vapor bubbles.

In relation to the heat transfer efficiency from the evaporator's wall, a characteristic M-shaped distribution, related to the vapor quality, should be expected in mini-geometries. An exemplary M-shaped pattern is shown in Figure 18.
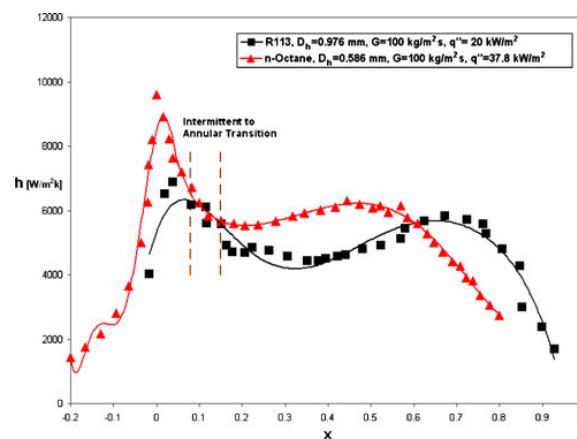

Figure 18. Two-phase flow characteristic M-shaped variation of the heat transfer coefficient [31].

The typical M-shape contains two clear maxima of the heat transfer coefficient—one for the quality x corresponding to about 0.1 and the second one for x of the order of 0.6–0.8. These maxima are associated with the changes in boiling mechanisms and flow structures [31]. In the presented case, the two main transitions can be marked out—from bubbly flow to a slug flow and from annular flow to a dryout. The full transition from the subcooled boiling, through the bubbly, slug and churn structures, can be seen in Figure 23 (left). As mentioned above, in the case of the thermosiphon discussed here, as regards the overall efficiency of heat transport, the resultant of two processes occurs. This is taken into account in Figure 19, showing the amount of heat taken from the evaporator's wall as a function of the vapor quality.

It can be seen that the first maximum occurs for a similar value of quality x, i.e., at the level of 0.1. It is beneficial both from the point of view of the heat exchange and from the point of view of the vapor lifting of the liquid (mass transport). The second maximum does not manifest itself so clearly, because the overall efficiency is negatively affected by the reduced efficiency of mass transport. The mass flux in the function of vapor quality is shown in Figure 20.
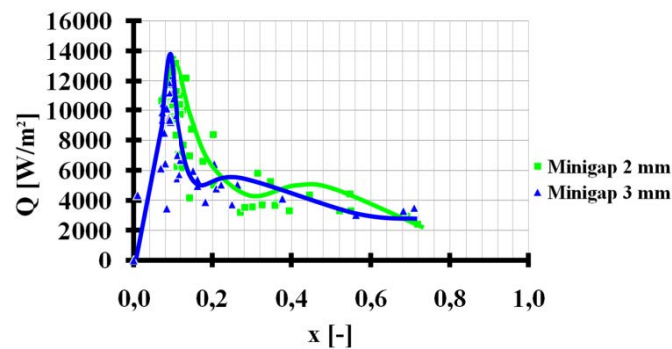
Figure 19. "M-shape" distribution of heat flux taken from the minigap wall as a function of vapor quality (test fluid: water).
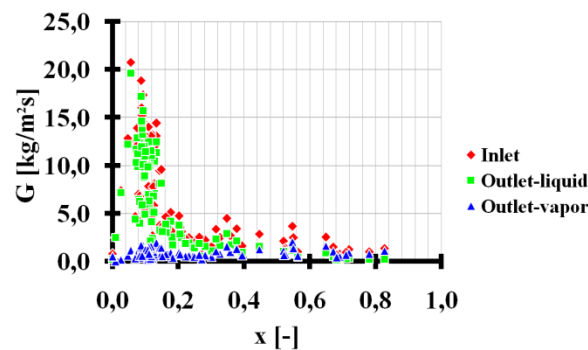

Figure 20. Mass flux of the test fluid (water) as a function of vapor quality.

Figure 21 shows the development of the boiling process depending on the wall superheating degree on the example of ethanol as the test fluid. A fully developed boiling occurs for a wall superheating >13 K and is accompanied by nucleation in the minigap space (see Figure 22). The clear structures can be distinguished, namely bubbly, slug and churn ones. Due to the very large ratio of the minigap width to its thickness, the annular structure (liquid on the wall, vapor in the middle) takes here a form of characteristic "foam" above the liquid line, as shown in Figure 16.

Figure 21. Flow boiling structures of ethanol for a different average wall superheating degree: **Left** = 1.53 K; **middle** = 13.22 K; **right** = 16.2 K.

A quite common case is the boiling present only in the manifolds for the proposed design of the minigap evaporator. This is facilitated by the bends of its construction and small horizontal walls, which are favorable to nucleation in these places. From the point of view of the vapor quality at the outlet of the evaporator and the degree of the wall superheating, the boiling is of the subcooled type.

If it occurs only in the outlet manifold, no flow structures are ever observed in the minigap—this may happen when an inlet medium temperature is much lower than the saturation temperature. Then, at the length of the minigap, the liquid is heated to a temperature close to saturation. When the evaporator inlet temperature is already close to the saturation temperature, it is possible that nucleation occurs also in the inlet manifold, while it's still not present at the wall of the minigap. The bubbles generated in the manifold simply pass through the minigap. Their shape could change as a result of changing the size of the channel. The vapor bubbles become flat, taking the form of slugs, but it is not strictly a boiling structure.
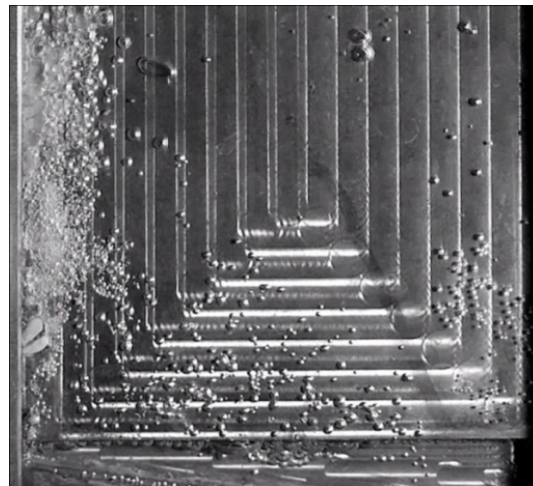

Figure 22. Vapor bubbles generated in active nucleation points on the minigap wall (2 mm).

An interesting example of this situation is shown in Figure 23. Because all thermosiphon settings are similar, only the test fluid properties are different—saturation temperature and heat capacity. For ethanol (wall superheating = 13.2 K), a fully-developed boiling is observed, including the nucleation on the wall. For water, nucleation occurs only in manifolds, whereas in the minigap the flow is almost adiabatic (wall superheating < 1 K).

As have been empirically found, as illustrated in Figures 19 and 20, all forms of sub-cooled boiling, even those with weakly visually visible flow structures (boiling only in the outlet manifold) ensure a fairly efficient operation of the system.
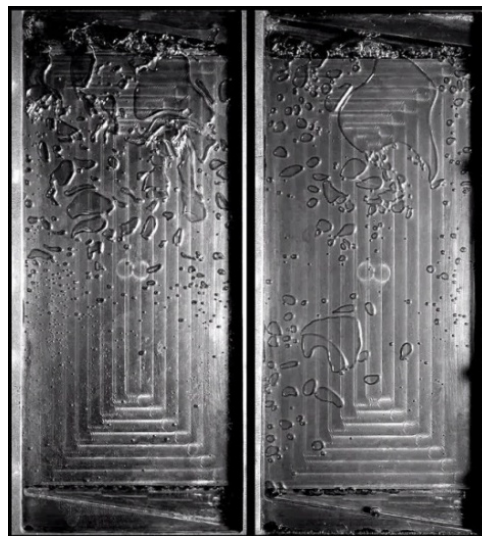

Figure 23. Comparison of the boiling process of ethanol (**left**) and water (**right**) for the same heat supplying parameters and equal system pressure.

3.6. Flow Maldistribution

In the case of using minigaps in installations, it is inevitable that the pipeline, usually cylindrical, needs to be transferred to a completely different geometry, with a very large difference between the two dimensions (width and depth). This issue is very similar to the problem of feeding the set of minichannels in a minichannel plate heat exchanger. Phenomena and problems occurring in such a system are also the subjects of other research [32]. Feeding the minichannel flow structure, as well as the minigap one, requires inlet and outlet collectors. The chosen method of solving this issue is important for the occurrence and specificity of maldistribution phenomenon. The authors decided to use the trapezoidal type of collectors (also called the "Z" design).

Figure 24 is representative of each case of the use of a water–air mixture and an adiabatic flow. The test fluid flowing from the inlet does not use the entire length of the inlet manifold but immediately flows into the space of the minigap. Therefore, the flow initially orientates near the "right" edge of the minigap. Later, the flow expands and ultimately achieves the outlet manifold over its entire length. In this way, "dead areas" occur, as well as an intensive reversed flows.

Figure 24. The way of flow distribution for an adiabatic flow of the water–air mixture.

As can be seen in Figure 25, the situation is completely different when the gas bubbles that force the flow are not supplied from an external source but vapor bubbles are generated by the evaporator itself. First of all, contrary to the situation shown in Figure 24, the flow generally has a tendency to orient itself closer to the left edge of the minigap. The effect of changing the minigap thickness is visible. For the largest thickness, the vapor bubbles move upwards in principle along a straight line, although the shift of the flow axis towards the left edge of the minigap is visible. Near the right edge, an increased tendency for reversed flows occurs (occasionally also in other places). As the thickness of the minigap decreases, the flow path of the vapor bubbles becomes more and more curved. For a thickness of 1 mm, it adopts the shape of the letter "S", with two distinct focal points of reversed flow.

It shows that the water–air model is not representative of the case of boiling flow. The complication of the test fluid distribution together with the increasing tendency to reversed flows may lead to the existence of some critical value of minigap thickness, below which these phenomena may affect the validity of its use. The thickness below which the minigap becomes ineffective was mentioned by Alam et al. [4].
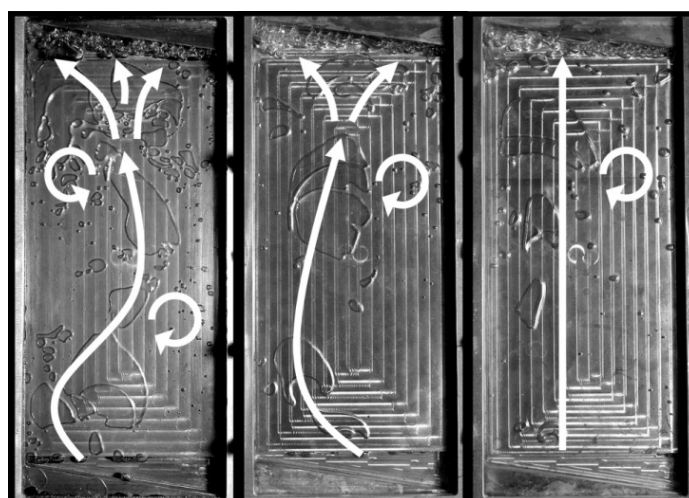
Figure 25. The way of flow distribution for the flow boiling for minigap thickness: **Left**—1 mm; **middle**—2 mm; **right**—3 mm.

3.7. The Uncertainty Analysis

Experimental uncertainty was determined using the sequential perturbation method of error analysis [34]. This method allows determining of the total experimental error by including errors originating from individual sources into the general database and averaging it using a root sum square method (RSS) (Equation (5)).

$$\text{RSS} = \sqrt{\sum_{i=1}^{n} \varepsilon_i^2} \tag{5}$$

The relative error is defined by Equation (6):

$$\sigma = \Delta y / y \tag{6}$$

where Δy is the absolute error and y is the measuring range.

Table 1 shows a detailed list of measurement uncertainties, calculated using method mentioned before. The overall inaccuracies should not exceed 4.24%.

Table 1. Partial experimental uncertainties.

Measured Number	Measuring Span	Absolute Error	Relative Error
Temperature (calibrated)	92 K	0.5 K	0.52%
Pressure	7×10^4 Pa	100 Pa	0.14%
Flow velocity—thermosiphon	1.66×10^{-5} m^3/s	4.16×10^{-7} m^3/s	2.5%
Flow velocity—heating circuit	8.33×10^{-6} m^3/s	2.5×10^{-7} m^3/s	3%
Linear dimensions	0.2 m	10^{-4} m	0.05%
Hydraulic diameter	0.013 m	10^{-4} m	0.76%
Heat flux	15,000 W/m^2	88.9 W/m^2	0.59%
Vapor quality	0.82	0.01	1.22%
Heat flux	15,000 W/m^2	88.9 W/m^2	0.59%
Vapor quality	0.82	0.01	1.22%

4. Discussion

On the basis of the conducted research, the following conclusions can be drawn.

1. It was shown that the filling level of the circuit influences the efficiency of the system operation. The thermosiphon with the filling level that does not provide liquid inside the separator's tube

works very poorly or does not work at all. It is crucial to obtain the vapor lifting effect inside the separator's tube. The vapor lifting of the liquid also works when the separator's tube is completely sunk. However, the filling level is not a critical parameter when the separator's tube is partially filled with the fluid—the system works effectively despite the total test fluid volume changes up to 23%.

2. Decreasing the minigap thickness leads to an intensification of the boiling process in the evaporator, but this does not mean a parallel, linear increase in system efficiency. The intensity of heat transfer as a function of vapor quality shows local maxima, according to the M-shape curve, while the maximum mass transport efficiency coincides with the first maximum of this curve, of about $x = 0.1$. The effective area of system operation also includes the range of subcooled boiling.

3. In contrast to pump-based systems, in the presented system, the minigap does not constitute a traditionally understood flow resistance because it generates pumping power itself. So, the flow resistance does not limit the possibility of reducing the thickness and hydraulic diameter of the minigap. However, there are other phenomena whose escalation along with the thickness reduction may be an obstacle here, i.e., escalation of flow maldistribution, reversed flows, or an early dryout occurrence.

4. The evaporator–condenser system shows the pulse/cyclic working nature of the system. Despite this, the temperature distributions in the evaporator and the condenser remain fixed over time.

5. The system shows an ability of dynamic self-regulation to the amount of transported heat, while the boundary parameters, i.e., the inlet and outlet temperatures in the evaporator and condenser remain constant. This is very beneficial from the application point of view when the amounts of transferred heat show large fluctuations—for example, in solar installations.

6. Increasing the heat flux in the evaporator increases the mass flux of the test fluid in the installation. This increase becomes more intense as the thickness of the minigap decreases.

7. The occurrence of a dry-out causes an immediate stop of the circulation and filing of the evaporator with a cold liquid coming from the condenser, so the system has the ability to self-terminate the dry-out. This is a particularly advantageous feature from the application point of view, as it significantly reduces the risk of a major burn-out failure.

8. When supplying the gas phase from the external source, e.g., by injecting into the evaporator inlet channel, the flow structures of such a mixture are not identical to those in the flow boiling.

9. Due to the complexity of mutual correlations between various parameters of the thermosiphon operation, as well as due to the mechanisms of its dynamic self-regulation, it is difficult to correlate the specific boiling structures with the optimal operating point of the entire system. However, the maximum heat transfer points can be indicated (according to the M-shape curve) as well as the point of maximum mass transfer.

10. With the transition from a cylindrical pipeline to minigap geometry, there is a need to arrange manifolds, which causes the risk of maldistribution phenomena, the occurrence of the dead zones, and areas of reversed flow.

Author Contributions: Conceptualization, M.K. and D.M.; Data curation, P.D.; Formal analysis, M.K.; Funding acquisition, M.K.; Investigation, M.K. and P.D.; Methodology, M.K.; Project administration, M.K.; Resources, M.K. and D.M.; Software, P.D.; Supervision, D.M.; Validation, M.K. and P.D.; Visualization, P.D.; Writing—original draft, M.K.; Writing—review & editing, P.D. and D.M.

Conflicts of Interest: The authors declare no conflict of interest.

References

1. Alam, T.; Lee, P.S.; Yap, C.R.; Jin, L. A comparative study of flow boiling heat transfer and pressure drop characteristics in microgap and microchannel heat sink and an evaluation of microgap heat sink for hotspot mitigation. *Int. J. Heat Mass Transf.* **2013**, *58*, 335–347. [CrossRef]
2. Bar-Cohen, A.; Holloway, C.; Kaffel, A.; Riaz, A. Waves and instabilities in high quality adiabatic flow in microgap channels. *Int. J. Multiph. Flow* **2016**, *83*, 62–76. [CrossRef]
3. Tamanna, A.; Lee, P.S. Flow boiling instability characteristics in expanding silicon microgap heat sink. *Int. J. Heat Mass Transf.* **2015**, *89*, 390–405. [CrossRef]
4. Alam, T.; Lee, P.S.; Yap, C.R.; Jin, L. Experimental investigation of local flow boiling heat transfer and pressure drop characteristics in microgap channel. *Int. J. Multiph. Flow* **2012**, *42*, 164–174. [CrossRef]
5. Ajith Krishnan, R.; Balasubramanian, K.R.; Suresh, S. Experimental investigation of the effect of heat sink orientation on subcooled flow boiling performance in a rectangular microgap channel. *Int. J. Heat Mass Transf.* **2018**, *120*, 1341–1357. [CrossRef]
6. Strąk, K.; Piasecka, M.; Maciejewska, B. Spatial orientation as a factor in flow boiling heat transfer of cooling liquids in enhanced surface minichannels. *Int. J. Heat Mass Transf.* **2018**, *117*, 375–387. [CrossRef]
7. Piasecka, M.; Maciejewska, B. Heat transfer coefficient during flow boiling in a minichannel at variable spatial orientation. *Exp. Therm. Fluid Sci.* **2015**, *68*, 459–467. [CrossRef]
8. Khodabandeh, R.; Furberg, R. Heat transfer, flow regime and instability of a nano- and micro-porous structure evaporator in a two-phase thermosyphon loop. *Int. J. Therm. Sci.* **2010**, *49*, 1183–1192. [CrossRef]
9. Asrar, P.; Zhang, X.; Green, C.E.; Bakir, M.; Joshi, Y.K. Flow boiling of R245fa in a microgap with staggered circular cylindrical pin fins. *Int. J. Heat Mass Transf.* **2018**, *121*, 329–342. [CrossRef]
10. Zhang, J.F.; Joshi, Y.K.; Tao, W.Q. Single phase laminar flow and heat transfer characteristics of microgaps with longitudinal vortex generator array. *Int. J. Heat Mass Transf.* **2017**, *111*, 484–494. [CrossRef]
11. Dai, X.; Yang, F.; Fang, R.; Yemame, T.; Khan, J.A.; Li, C. Enhanced single-and two-phase transport phenomena using flow separation in a microgap with copper woven mesh coatings. *Appl. Therm. Eng.* **2013**, *54*, 281–288. [CrossRef]
12. Piasecka, M. Impact of selected parameters on refrigerant flow boiling heat transfer and pressure drop in minichannels. *Int. J. Refrig.* **2015**, *56*, 198–212. [CrossRef]
13. Nasr, M.H.; Green, C.E.; Kottke, P.A.; Zhang, X.; Sarvey, T.E.; Joshi, Y.K.; Bakir, M.S.; Fedorov, A.G. Flow regimes and convective heat transfer of refrigerant flow boiling in ultra-small clearance microgaps. *Int. J. Heat Mass Transf.* **2017**, *108*, 1702–1713. [CrossRef]
14. Cieslinski, J.T. Effect of nanofluid concentration on two-phase thermosyphon heat exchanger performance. *Arch. Thermodyn.* **2016**, *37*, 23–40. [CrossRef]
15. Saad, I.; Maalej, S.; Zaghdoudi, M.C. Combined effects of heat input power and filling fluid charge on the thermal performance of an electrohydrodynamic axially grooved flat miniature heat pipe. *Appl. Therm. Eng.* **2018**, *134*, 469–483. [CrossRef]
16. Narcy, M.; Lips, S.; Sartre, V. Experimental investigation of a confined flat two-phase thermosyphon for electronics cooling. *Exp. Therm. Fluid Sci.* **2018**, *96*, 516–529. [CrossRef]
17. Panse, S.S.; Kandlikar, S.G. A thermosiphon loop for high heat flux removal using flow boiling of ethanol in OMM with taper. *Int. J. Heat Mass Transf.* **2017**, *106*, 546–557. [CrossRef]
18. Klugmann, M.; Dąbrowski, P.; Mikielewicz, D. Selected thermal and flow issues in a reversed thermosiphon with a steam liquid lifter. *E3S Web Conf.* **2018**, *70*, 02009. [CrossRef]
19. Dobriansky, Y. Concepts of self-acting circulation loops for downward heat transfer (reverse thermosiphons). *Energy Convers. Manag.* **2011**, *52*, 414–425. [CrossRef]
20. Roberts, C.C. A review of heat pipe liquid delivery concepts. *J. Heat Recover. Syst.* **1981**, *1*, 261–266. [CrossRef]
21. Duffie, J.A.; Beckman, W.A. *Solar Engineering of Thermal Processes*; John Wiley & Sons: Hoboken, NJ, USA, 2013; ISBN 0470873663.
22. Basu, D.N.; Bhattacharyya, S.; Das, P.K. A review of modern advances in analyses and applications of single-phase natural circulation loop in nuclear thermal hydraulics. *Nucl. Eng. Des.* **2015**, *280*, 326–348. [CrossRef]

23. Zhao, D.; Martini, C.E.; Jiang, S.; Ma, Y.; Zhai, Y.; Tan, G.; Yin, X.; Yang, R. Development of a single-phase thermosiphon for cold collection and storage of radiative cooling. *Appl. Energy* **2017**, *205*, 1260–1269. [CrossRef]

24. Tong, L.; Chen, J.; Cao, X.; Yang, S.; Liao, S.; Deng, J.; Zeng, W. Visualization experiments on the geyser boiling-induced instability in vertical circular tube at low-pressures. *Ann. Nucl. Energy* **2015**, *77*, 487–497. [CrossRef]

25. Smyth, M.; Quinlan, P.; Mondol, J.D.; Zacharopoulos, A.; McLarnon, D.; Pugsley, A. The experimental evaluation and improvements of a novel thermal diode pre-heat solar water heater under simulated solar conditions. *Renew. Energy* **2018**, *121*, 116–122. [CrossRef]

26. Li, T.; Jiang, Y.; Li, Z.; Liu, Q.; Tang, D.W. Loop thermosiphon as a feasible cooling method for the stators of gas turbine. *Appl. Therm. Eng.* **2016**, *109*, 449–453. [CrossRef]

27. Dhumane, R.; Mallow, A.; Qiao, Y.; Gluesenkamp, K.R.; Graham, S.; Ling, J.; Radermacher, R. Enhancing the Thermosiphon-Driven Discharge of a Latent Heat Thermal Storage System used in a Personal Cooling Device. *Int. J. Refrig.* **2018**, *88*, 599–613. [CrossRef]

28. He, T.; Mei, C.; Longtin, J.P. Système de refroidissement assisté par thermosiphon pour les applications frigorifiques. *Int. J. Refrig.* **2017**, *74*, 163–174.

29. Goedecke, R.; Scholl, S. Enlarged operation ranges for thermosiphon reboilers using pillow plates. *Chem. Eng. Res. Des.* **2015**, *99*, 58–66. [CrossRef]

30. Dobriansky, Y.; Yohanis, Y.G. Cyclical reverse thermosiphon. *Arch. Thermodyn.* **2010**, *31*, 3–32. [CrossRef]

31. Bar-Cohen, A.; Sheehan, J.R.; Rahim, E. Two-Phase Thermal Transport in Microgap Channels—Theory, Experimental Results, and Predictive Relations. *Microgravity Sci. Technol.* **2012**, *24*, 1–15. [CrossRef]

32. Mikielewicz, D.; Klugmann, M.; Wajs, J. Experimental Investigation of M-Shape Heat Transfer Coefficient Distribution of R123 Flow Boiling in Small-Diameter Tubes. *Heat Transf. Eng.* **2012**, *33*, 584–595. [CrossRef]

33. Dąbrowski, P.; Klugmann, M.; Mikielewicz, D. Selected studies of flow maldistribution in a minichannel plate heat exchanger. *Arch. Thermodyn.* **2017**, *38*, 135–148. [CrossRef]

34. Moffat, R.J. Describing the uncertainties in experimental results. *Exp. Therm. Fluid Sci.* **1988**, *1*, 3–17. [CrossRef]